Engineering Failure Analysis 61 (2016) 69–76

Contents lists available at ScienceDirect

Engineering Failure Analysis

journal homepage: www.elsevier.com/locate/efa

Degradation of mechanical and corrosion resistance properties of AISI 317L steel exposed at 550 °C

H.N. Farneze [a], S.S.M. Tavares [a,*], J.M. Pardal [a], R.F. do Nascimento [b], H.F.G. de Abreu [c]

[a] Universidade Federal Fluminense, Escola de Engenharia, Rua Passo da Pátria, 156, CEP 24210-240, Niterói, RJ, Brazil
[b] NUCLEP, Departamento de Engenharia Metalúrgica e Materiais, Brazil
[c] Universidade Federal do Ceará, Departamento de Engenharia Metalúrgica e Materiais, Brazil

ARTICLE INFO

Article history:
Received 29 September 2014
Accepted 31 August 2015
Available online 5 September 2015

Keywords:
AISI 317L
Aging
Pitting corrosion
Deleterious phases

ABSTRACT

The use of austenitic stainless steel type AISI 317L has increased in the last years, in substitution to AISI 316L and other austenitic grades. The higher Mo content (3.0 wt.%. at least) gives higher corrosion resistance to AISI 317L. However, some concern arises when this material is selected to high temperature process services in refineries. Microstructural changes such as chromium carbide precipitation and sigma phase formation may occur in prolonged exposure above 450 °C. In this work, the microstructure evolution of AISI 317L steel during aging at 550 °C was analyzed. Thermodynamic calculations with Thermocalc® and detailed microstructural analysis were performed in steel plate base metal and in weld metal produced by GTAW process. The aging for 200, 300 and 400 h promoted gradual embrittlement and deterioration of corrosion resistance of both weld and base metal. The results show that the selection of AISI 317L steel to services where temperatures can reach 550 °C is not recommended.

1. Introduction

Austenitic stainless steels can be selected to high temperature services due to its high creep and oxidation resistance. However, microstructural changes may take place during service. AISI 304 and 304 H steels undergo sensitization due to $Cr_{23}C_6$ precipitation between 450 and 850 °C [1]. AISI 304L is also susceptible to sensitization, but, due to its lower carbon (less than 0.03% C), the kinetics of precipitation is much lower, and the amount of chromium carbides that can be formed is smaller than in 304 and 304 H grades. Nevertheless, "H" grades are often selected for high temperature services because Cr carbides enhance creep resistance [2].

If sensitization by $Cr_{23}C_6$ precipitation is considered a problem for some application where corrosion resistance must be maintained, Nb or Ti-stabilized steels can be used (grades AISI 347 or AISI 321). These steels must be correctly heat treated (stabilization at ~900 °C), as discussed elsewhere [3–4].

Some austenitic stainless steels are also susceptible to sigma (σ) phase formation. Weld and base metal of AISI 321 and 347 undergone σ phase precipitation at 700 °C [5]. Källqvist and Andrén [6] investigated the precipitation in Nb stabilized AISI 347 aged at 500 °C, 600 °C and 700 °C for long periods (>45,000 h). σ-phase particles were formed at all the aging temperatures and the volume fraction increased with increasing aging temperature.

The increase of Cr, Mo and Si and other ferritizing elements accelerates the precipitation of σ phase. The precipitation via δ-ferrite is more rapid because this phase is Cr, Mo and Si enriched, and also because the diffusion coefficients in the bcc phase are much higher than in the fcc austenite. As a consequence, weld metals and cast pieces of conventional austenitic stainless steels are more susceptible to σ phase precipitation than base metals, since a higher amount of δ ferrite is usually found in the cast structure.

* Corresponding author.
E-mail address: ssmtavares@terra.com.br (S.S.M. Tavares).

http://dx.doi.org/10.1016/j.engfailanal.2015.08.044
1350-6307/

Table 1
Chemical compositions of base and weld metals.

Material	C	Mn	Si	S	P	Cr	Ni	Mo
Base metal	0.024	1.34	0.47	0.003	0.031	18.13	11.41	3.02
Weld metal	0.008	1.63	0.61	0.003	0.028	18.26	13.63	3.08

AISI 316L and AISI 310 steels are particularly susceptible to sigma phase precipitation. AISI 310 is free from delta ferrite, but the high Cr content (~24%) favors the σ precipitation. The sequence of precipitation $\gamma \rightarrow M_{23}C_6 \rightarrow \sigma$ was proposed [7]. In AISI 316L the addition of 2–3% Mo increases the pitting resistance but enhances the kinetics of σ phase precipitation.

Recently, due to the demand of higher pitting corrosion resistance materials, AISI 317L steel with 3–4% Mo have been selected instead of AISI 316L. Mo addition increases the resistance to naphthenic corrosion, which is a serious problem in distillation towers. Some applications of AISI 317L steel in oil refineries are clads, vessels, tubes, valves and accessories. For some of these applications the service temperature can reach 550 °C or higher.

Although some previous works have predicted structural and property changes on AISI 316/316L steel subjected to aging [8–10], very few articles were published with AISI 317L. In this work the influence of long term exposition in the microstructure, mechanical and corrosion properties of AISI 317L steel was investigated.

Austenitic steels without δ ferrite are also susceptible. In fully austenitic weld metal sigma phase precipitation can start at austenite–austenite grain boundaries.

2. Methodology

Plates of AISI 317L steel with 8 mm of thickness were welded by GTAW process with 7 passes. Heat input was limited to the interval of 0.8–1.0 kJ/mm, and maximum inter-pass temperature was 150 °C. After welding the chemical composition of weld metal was determined by plasma spectroscopy.

Samples from the base metal were cut with dimensions 8 × 12 × 60 mm. Welded joints were also cut with approximately the same dimensions, but some angular distortion was produced by welding. The samples were heat treated at 550 °C for 200 h, 300 h and 400 h in a resistance furnace, followed by water cooling.

Sub-size specimens (5 mm) for Charpy impact tests with V notch were machined from base metal and welded joint. The notches of specimens from the welded joint were placed in the center line of the weld metal. Impact tests were carried out at room temperature in a universal machine with 300 J of capacity.

Cyclic polarization tests in 3.5% NaCl solution were used to evaluate the pitting corrosion resistance. The test is described in the ASTM G-61 standard [11]. A three electrodes cell, with working electrode of the material analyzed, reference and counter-electrode was used. Working electrodes were prepared with the specimen to be analyzed embedded in epoxy resin among with a cooper wire for electric contact. Saturated calomel electrode was used as reference and a Pt wire was used as counter-electrode. The tests were conducted with the solution at 22 °C. After the stabilization of the open circuit potential (E_{OCP}) the anodic polarization with sweep rate 1 mV/s was initiated. The sweeping was reverted to the cathodic direction when the current density achieved 1 mA/cm^2. The parameters obtained from the polarization curves were the open circuit potential after 1 h (E_{OCP}), the pitting potential (E_{PIT}) and the repassivation potential (E_{RP}).

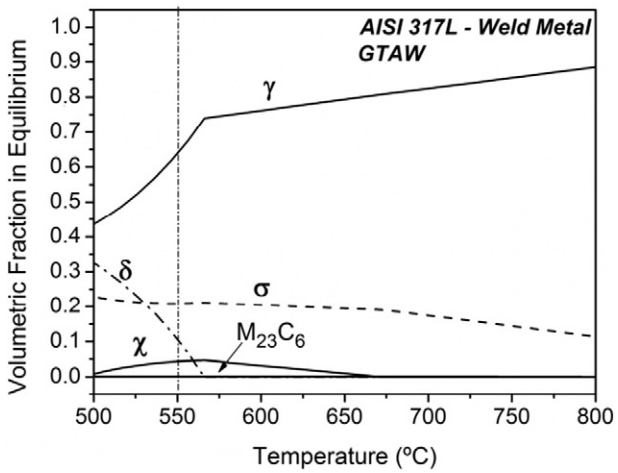

Fig. 1. Equilibrium phase volume fractions as function of temperature determined by computational thermodynamics.

Table 2
Phase composition and volume fraction predictions from Thermocalc® to weld and base metals aged at 550 °C.

	Phase	Volume fraction
Base metal	γ	0.4889
	δ	0.2724
	σ	0.1781
	χ	0.0549
	$M_{23}C_6$	0.0057
Weld metal	γ	0.6415
	δ	0.1032
	σ	0.2095
	χ	0.0440
	$M_{23}C_6$	0.0018

Microstructural evolution was evaluated by light optical (LOM) and electronic microscopy (SEM). Specimens for LOM were electrolytically etched in 10% KOH solution with 3 V by 20 s. Specimens for SEM were carefully polished till 1 μm diamond paste and observed in the backscattered electrons mode.

Electron backscattered electrons diffraction (EBSD) was used to identify the phases precipitated in the specimen of weld metal aged at 550 °C for 400 h. For this analysis a Field Emission Gun Scanning Electron Microscope (FEG-SEM) FEI QUANTA 400 was used. The specimen was gingerly polished in colloidal silica.

Magnetic analysis with ferritoscope Helmut Fischer® was used to measure the delta ferrite content. Thermocalc® simulation with TCFE3 database was used to predict the phases more stable at 550 °C.

3. Results and discussion

Table 1 shows the chemical compositions of base metal and weld metal. The Cr, Ni, Mo and C contents were used as input to Thermocalc® simulation. The results for weld metal are shown in Fig. 1. Table 2 shows the equilibrium volume fractions of austenite (γ), ferrite (δ), sigma (σ), chi (χ) and $Cr_{23}C_6$ in base and weld metals.

The microstructure of un-aged base metal consists of austenite and delta ferrite, as shown in Fig. 2(a–b). The weld metal also contains some elongated ferrite islands, as shown in Fig. 3(a). However, a detailed SEM image of the un-aged weld metal suggests that Mo-rich particles were precipitated during welding (Fig. 3(b)). In backscattered electrons image the Mo-rich precipitates are bright because Mo is heavier than Fe, Ni and Cr. The EDS analysis of the precipitates is compared to typical ferrite and austenite analysis in Table 3, but it is rather qualitative because the particles are too fine to be analyzed without the influence of the surrounding matrix.

The ferrite volume fractions measured with the ferritoscope were 7.1 ± 0.9% and 4.0 ± 0.5% in weld metal and base metal, respectively. Fig. 4 shows the variation of the ferrite volume fraction with aging time at 550 °C. The behavior indicates the transformation of ferrite into paramagnetic phases, which can be γ and intermetallic phases. According to data of Fig. 1 the intermetallic phases are χ and σ. However, Yang and Busby [8] have found by thermodynamic calculation that Laves phase (Fe_2Mo) was prone to precipitate among with σ, δ, χ and $M_{23}C_6$ in an AISI 316 stainless steel with 2.33% Mo and 16.6% Cr treated at 550 °C.

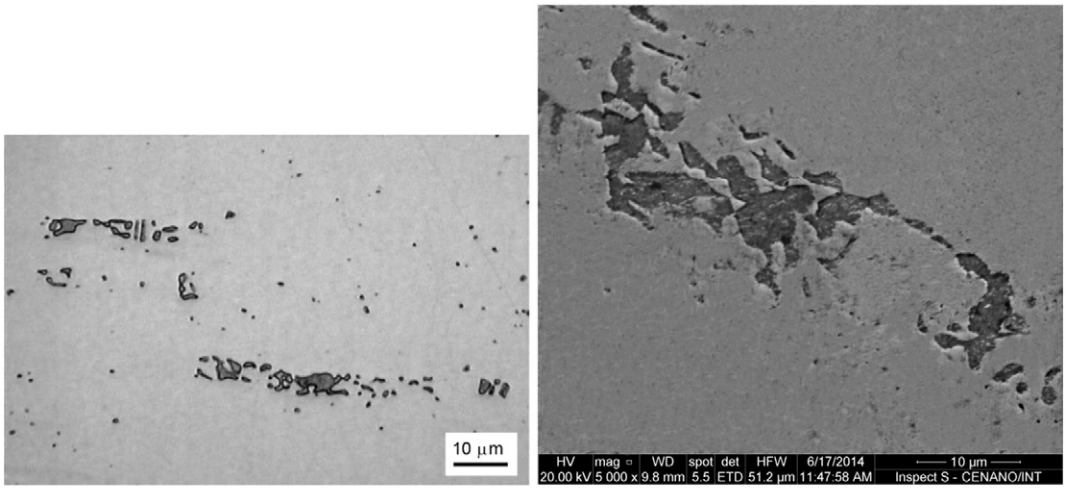

Fig. 2. Microstructure of un-aged base metal: (a) LOM image; (b) SEM backscattered electrons image.

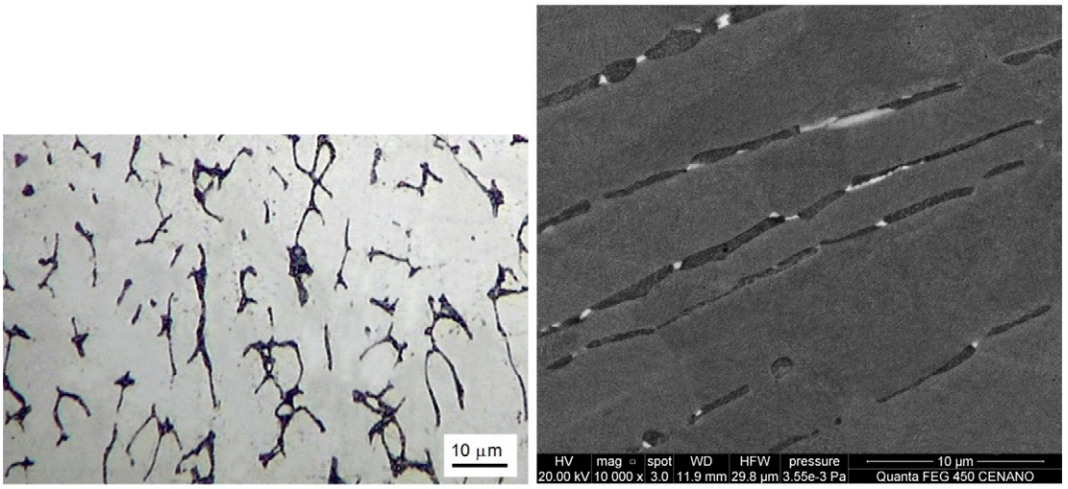

Fig. 3. Microstructure of un-aged weld metal: (a) LOM image; (b) SEM backscattered electron image.

Table 3
EDS analysis of phases observed in the un-aged welded metal.

Region	Cr	Ni	Mo
Ferrite (δ)	24.54	6.33	4.30
Austenite (γ)	20.00	10.37	2.68
Bright precipitates	24.60	5.78	7.60

The decomposition of ferrite at 550 °C can be observed by microscopy, as shown in Fig. 5(a) for base metal and (b) for weld metal. EDS analysis of these precipitates could not be performed, since they are very fine and dispersed inside the ferrite islands. The small size of precipitates formed at 550 °C is attributed to the low diffusivity at this temperature. The identification and quantification of these precipitates were achieved by EBSD analysis. Fig. 6 shows the phases map obtained in the specimen of weld metal aged at 550 °C for 400 h. The intermetallic phases $Cr_{23}C_6$, σ and χ were identified and quantified at this condition (Table 4). Although the values measured are quite different from the Thermocalc prediction, it must be considered that the equilibrium conditions must have not been achieved.

The effects of the intermetallic precipitation at 550 °C can lead to the degradation of mechanical and corrosion resistance properties, which may cause catastrophic failures in service. The effect of the time of exposure at 550 °C on the impact toughness can be

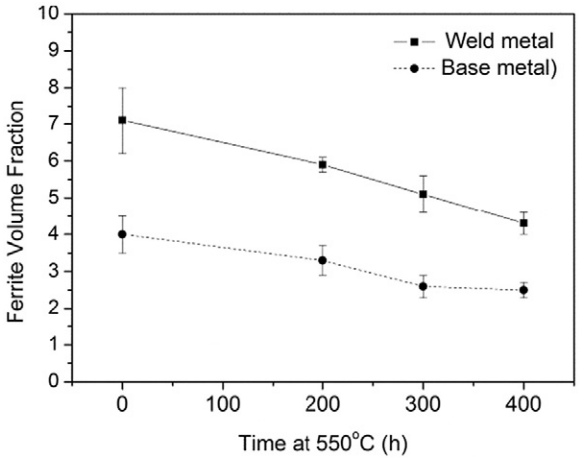

Fig. 4. Variation of volume fraction with time of exposure at 550 °C.

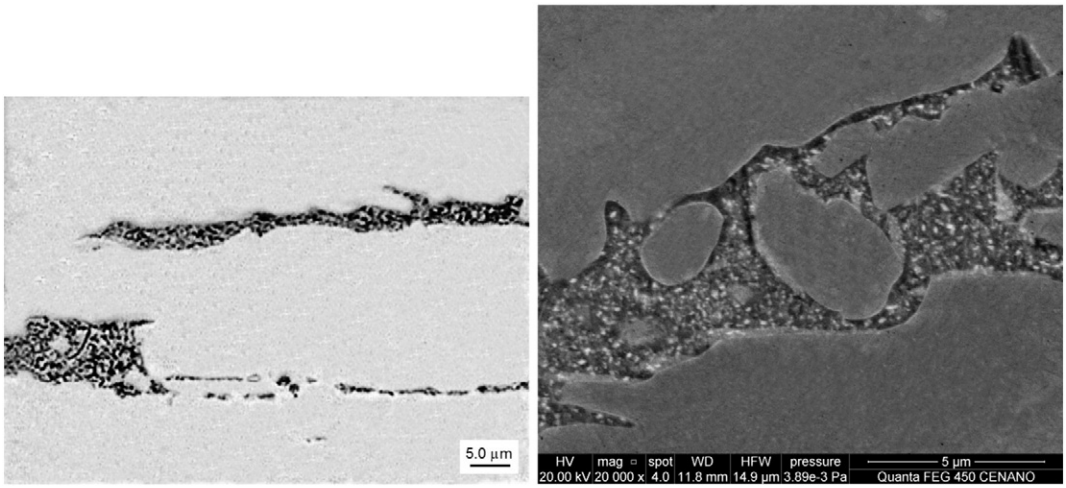

Fig. 5. Ferrite decomposition in specimens aged at 550 °C for 400 h: (a) base metal observed by LOM; (b) weld metal observed by SEM.

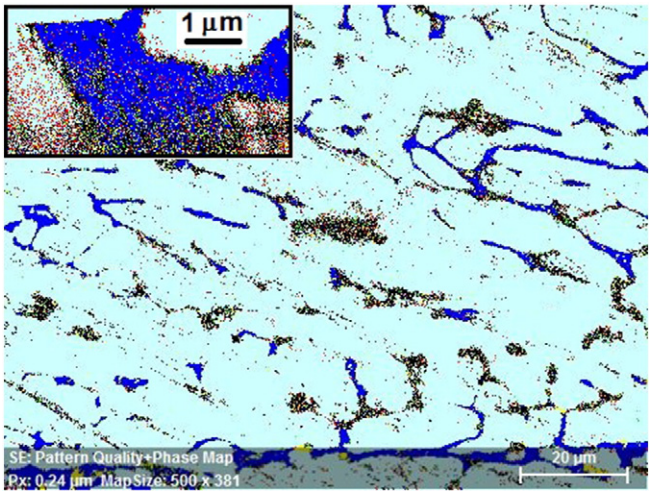

Fig. 6. Phase map of specimen of weld metal aged at 550 °C for 400 h.

observed in Fig. 7. First, it is observed that the toughness of un-aged base metal (109 J) is much higher than the un-aged weld metal (74 J). This can be attributed to the higher amount of ferrite and, mainly, to the Cr-rich precipitates found in the weld metal (see Fig. 3(b)). The overall decrease of weld metal and base metal toughness with the increase of time of exposition at 550 °C is consequence of the decomposition of ferrite into fine intermetallic precipitates, as shown in Fig. 5(a–b).

Figs. 8(a–b) and 9(a–b) show the images of the fracture surfaces of un-aged and aged (400 h–550 °C) weld metal, for comparison. The fracture surface of the specimen aged shows smaller dimples, which is a signal of the decrease of toughness. Besides this, particles of the intermetallic phases can be observed with high magnification (Fig. 9(b)).

Table 4
Amounts of phases determined by EBSD in the weld metal aged at 550 °C for 550 h.

Phase	Volumetric percentage
γ	90.63
δ	5.86
σ	1.43
χ	0.62
$Cr_{23}C_6$	1.46

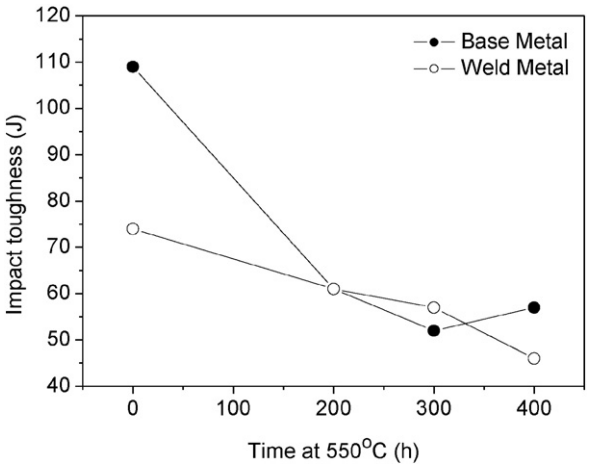

Fig. 7. Variation of the impact toughness with aging time at 550 °C.

The intermetallic phases also decrease the corrosion resistance of the AISI 317L steel. First, the polarization curves of samples of un-aged base metal and un-aged weld metal were compared in Fig. 10. The pitting (E_{PIT}) and repassivation (E_{RP}) potentials measured in the base metal are very close and around 1.0 V_{SCE}. These parameters were much inferior in the weld metal. In accordance, the hysteresis of the curve after the reversion of the potential also indicates a much lower pitting resistance of the weld metal sample. The explanation is again related to the presence of intermetallic compounds precipitated in the ferrite phase, which cause Cr and Mo depletion in a narrow region around them.

Table 5 shows the parameters obtained from the polarization curves, i.e., E_{OCP}, E_{PIT} and E_{RP} for specimens un-aged and aged at 550 °C. The higher the pitting potential and repassivation potential the higher is the pitting corrosion resistance of the material. The difference E_{PIT}–E_{OCP} represents the passivation interval of the material. The overall pitting resistance of the steel is decreased by the increase of aging time at 550 °C.

4. Conclusions

The effects of the exposure of the AISI 317L steel to 550 °C were studied. The initial microstructure of the base metal consisted of austenite and 4% of elongated islands of delta ferrite. The aging at 550 °C up to 400 h caused the decomposition of the ferrite phase into fine and dispersed intermetallic compounds, which caused the decrease of toughness and pitting corrosion.

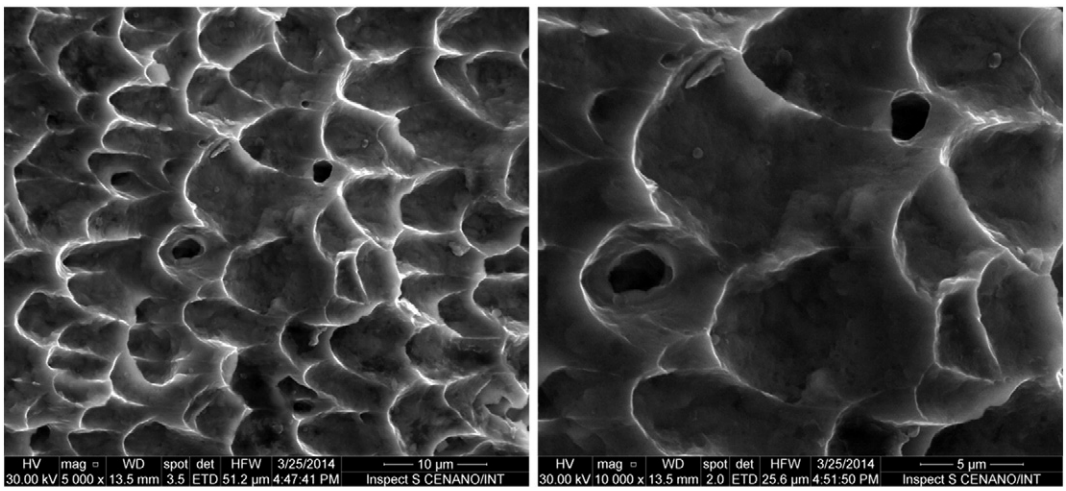

Fig. 8. Fractograph of un-aged weld metal after Charpy impact test.

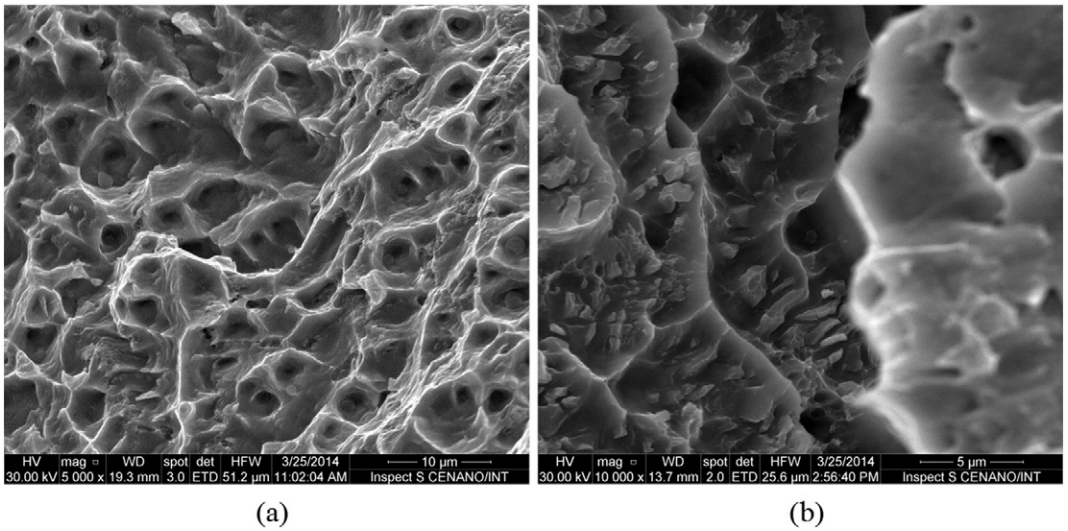

Fig. 9. Fractograph of weld metal aged 400 h at 550 °C after Charpy impact test.

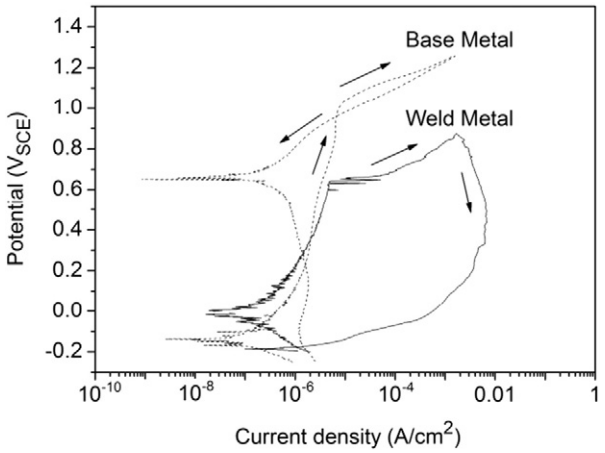

Fig. 10. Polarization curves of the un-aged base metal and weld metal.

The weld metal produced by GTAW showed a typical microstructure of austenite and 7.1% of delta ferrite. However, some intermetallic Mo-rich precipitates were found into the ferrite islands. As consequence, the toughness and corrosion resistance of the un-aged weld metal was inferior to the un-aged base metal.

The aging of the weld metal at 550 °C provoked a further decrease of pitting resistance and embrittlement. Similarly to the base metal, ferrite has decomposed into fine intermetallic phases precipitates. These precipitates were found in the fracture surface observed with high magnification.

The precipitates of $Cr_{23}C_6$, sigma (σ) and chi (χ) phases were identified by EBSD analysis of weld metal aged at 550 °C for 400 h. These phases were previewed by the Thermocalc® simulation.

Table 5
Parameters obtained from the polarization curves of base metal (BM) and weld metal (WM).

Region - condition	E_{OCP} (V_{SCE})	E_{PIT} (V_{SCE})	E_{RP} (V_{SCE})	$E_{PIT} - E_{OCP}$ (V_{SCE})
BM — as received	−0.14	1.03	0.96	1.17
BM — 550 °C–200 h	−0.16	1.02	<−0.16	1.18
BM — 550 °C–300 h	−0.30	0.82	<−0.30	1.12
BM — 550 °C–400 h	−0.20	0.63	<−0.20	0.83
WM — as received	−0.16	0.65	<−0.16	0.81
WM — 550 °C–200 h	−0.20	0.50	−0.19	0.70
WM — 550 °C–300 h	−0.16	0.48	<−0.16	0.64
WM — 550 °C–400 h	−0.27	0.43	<−0.27	0.70

Acknowledgments

Authors acknowledge the Brazilian research agencies CAPES (50/2011), CNPq (305294/2014-8), and FAPERJ (E-26/110.750/2012) for the financial support.

References

[1] C.A. Della Rovere, M. Castro-Rebello, S.E. Kuri, Corrosion behavior analysis of an austenitic stainless steel, Eng. Fail. Anal. Engineering Failure Analysis 31 (2013) 40–47.
[2] J.M.C. Farrar, A.W. Marshall, Type "300 h" austenitic stainless steel weld metals for high-temperature service, Proceedings of Stainless Steel World 99 Conference, KCI Publishing BV, The Hague 1999, pp. 147–162.
[3] A.Y. Kina, V.M. Souza, S.S.M. Tavares, J.A. Souza, H.F.G. de Abreu, Influence of heat treatments on the intergranular corrosion resistance of the AISI 347 cast and weld metal for high temperature services, J. Mater. Process. Technol. 199 (2008) 391–395.
[4] V. Moura, A.Y. Kina, S.S.M. Tavares, L.D. Lima, F.B. Mainier, Influence of stabilization heat treatments on microstructure, hardness and intergranular corrosion resistance of the AISI 321 stainless steel, J. Mater. Sci. 43 (2008) 536–540.
[5] K. Guan, X. Xu, H. Xu, Z. Wang, Effect of aging at 700 °C on precipitation and toughness of AISI321 and AISI 347 austenitic stainless steel welds, Nucl. Eng. Des. 235 (2005) 2485–2494.
[6] J. Källqvist, H.-O. Andrén, Microanalysis of a stabilised austenitic stainless steel after long term ageing, Mater. Sci. Eng. A270 (1999) 27–32.
[7] S.S.M. Tavares, J.M. Pardal, S.S. Carvalho, Barbosa C, failure analysis of AISI 310S plate in an inert gas generator used in off-shore oil platform, Eng. Fail. Anal. 18 (2011) 1435–1444.
[8] Y. Yang, J.T. Busby, Thermodynamic modeling and kinetics simulation of precipitate phases in AISI 316 stainless steels, J. Nucl. Mater. 448 (1–3) (2014) 282–293.
[9] H. Sahlaoui, H. Sidhom, Experimental investigation and analytical prediction of σ-phase precipitation in AISI 316L austenitic stainless steel, Metall. Mater. Trans. A 44A (2013) 3077–3083.
[10] K. Chandra, V. Kain, V. Bhutani, V.S. Raja, R. Tewari, G.K. Dey, J.K. Chakravartty, Low temperature thermal aging of austenitic stainless steel welds: kinetics and effects on mechanical properties, Mater. Sci. Eng. A 534 (2012) 163–175.
[11] ASTM G-61–09, Standard Test Method for Conducting Cyclic Potentiodynamic Polarization Measurements for Localized Corrosion Susceptibility of Iron-, Nickel-, or Cobalt-Based-Alloys, American Society for Testing and Materials, Philadelphia/USA, 2009.